ORIGINAL PAPER

physica status solidi a pss

www.pss-a.com

Improved Efficiency of Ultraviolet B Light-Emitting Diodes with Optimized p-Side

Tim Kolbe, Arne Knauer, Jens Rass, Hyun Kyong Cho, Anna Mogilatenko, Sylvia Hagedorn, Neysha Lobo Ploch, Sven Einfeldt, and Markus Weyers*

The effects of design and thicknesses of different optically transparent p-current spreading layers [short-period superlattice, superlattice (SL), and bulk p-$Al_{0.38}Ga_{0.62}N$] as well as the type and thickness of the p-GaN cap layer on the electrical and optical characteristics of 310 nm ultraviolet light-emitting diodes (LEDs) are investigated. Scanning transmission electron microscopy measurements display self-organized composition variations in the nonpseudomorphically grown SLs, reducing the effect of increased hole injection efficiency of a SL. In addition, the effect leads to an increased operation voltage. In contrast, the bulk p-AlGaN layer has a uniform composition and the corresponding LEDs show only a slightly lower output power along with a lower operating voltage. If the thickness of the p-AlGaN bulk layer in the LED is reduced from 150 nm to 50 nm, the output power increases and the operating voltage decreases. Finally, LEDs with a nonuniform p^+-GaN cap layer from a 3D island-like growth mode feature the highest output power and operating voltage. In contrast, the output power and operating voltage of LEDs with a smooth and closed cap depend on the thickness of p^+-GaN. The highest output power and lowest operating voltage are achieved for LEDs with the thinnest p^+-GaN cap.

1. Introduction

The development of efficient ultaviolet B (UVB) light-emitting diodes (LEDs) based on the (In)AlGaN material system is essential to leverage their vast commercial potential. UVB LEDs are expected to not only replace traditional mercury lamps in applications such as curing of polymers and phototherapy but also establish new applications in the fields of plant growth and sensing.[1,2] However, despite the enormous progress that UVB LEDs have made, the performance characteristics of these devices still suffer from low efficiencies due to high defect densities and a poor carrier injection compared with LEDs operating in the visible wavelength range.[3–5] Today, the best UVB LEDs exhibit external quantum efficiencies of only a few percent.[6–11]

The optimization of the current spreading layers, the active region, the electron blocking layer (EBL), and the contact layers is very important to improve the power and operating voltage of UV LEDs. We have previously extensively discussed the influence of the n-layer heterostructure design,[12] the quantum-well (QW) and quantum-barrier composition,[13] the QW numbers,[14] and the QW width[15] as well as the EBL design[16,17] on the emission characteristics and efficiency of UV LEDs. The p-layer heterostructure design and the p-doped cap layer are further key challenges to realize efficient UV LEDs with a low operating voltage. Therefore, in the majority of cases, an optically transparent p-doped bulk AlGaN layer or an AlGaN/AlGaN short-period superlattice (SPSL) (to enhance the ionization of magnesium acceptors by polarization fields) in combination with a p^+-GaN cap layer[18,19] is used in UVB and ultraviolet C (UVC) LEDs to realize layers with a high conductivity and minimal contact resistivity. In previous studies also other concepts have been realized, for example, a thick absorbing p-GaN layer,[20] a fully transparent p-side consisting of an AlGaN layer[8,21] without any p-GaN cap, or the use of an AlGaN/AlN SPSL.[22,23]

In this article, we will present a systematic investigation of the influence of the design [SPSL vs. superlattice (SL) versus bulk p-$Al_{0.38}Ga_{0.62}N$] and the thickness of the bulk p-$Al_{0.38}Ga_{0.62}N$ current spreading layer as well as the morphology and thickness of the p^+-GaN cap layer on the optical power and operating voltage of 310 nm LEDs. To realize the optical transparency of the

Dr. T. Kolbe, Dr. A. Knauer, Dr. J. Rass, Dr. H. K. Cho, Dr. A. Mogilatenko, Dr. S. Hagedorn, Dr. N. Lobo Ploch, Dr. S. Einfeldt, Prof. M. Weyers
Ferdinand-Braun-Institut
Leibniz-Institut für Höchstfrequenztechnik
Gustav-Kirchhoff-Strasse 4, 12489 Berlin
E-mail: tim.kolbe@fbh-berlin.de

Dr. T. Kolbe, Dr. J. Rass, Dr. N. Lobo Ploch
UVphotonics NT GmbH
Gustav-Kirchhoff-Strasse 4, 12489 Berlin

Dr. A. Mogilatenko
Institute of Physics
Humboldt University of Berlin
Newtonstrasse 15, 12489 Berlin

The ORCID identification number(s) for the author(s) of this article can be found under https://doi.org/10.1002/pssa.202000406.

Correction added on 10 September 2020, after first online publication: Projekt Deal funding statement has been added.

DOI: 10.1002/pssa.202000406

physica status solidi a
www.pss-a.com

p-current spreading layer for the 310 nm emission wavelength, its average aluminum mole fraction was set to 38%. The resistivity of the p-side current spreading layer in our UVB LEDs is expected to be significantly larger than in UVA LEDs where the corresponding aluminum mole fraction is below 25%. In contrast, for an aluminum mole fraction below 60%, high compressive strain and nonpseudomorphic growth on the AlN/sapphire template are to be expected. Thus, electro-optical performance will be discussed in combination with scanning transmission electron microscopy (STEM) and scanning electron microscopy (SEM) measurements, giving information on the structural properties.

2. Results and Discussion

In the next three subsections, the effect of design and the thickness of the current spreading layer as well as the growth conditions and thickness of the p^+-GaN cap layer on the emission characteristics of 310 nm UV LEDs are discussed. It should be noted that only the samples of one subsection were grown on the same LED template batch and processed in the same batch, so that only LEDs from one subsection can be compared directly with each other.

2.1. Design of p-Current Spreading Layer

In a first series of samples, the influence of the p-current spreading layer design was investigated. Therefore, LEDs with a nonpseudomorphic nominally 30-period SPSL or 6-period p-$Al_{0.42}Ga_{0.58}N/Al_{0.32}Ga_{0.68}N$ SL as well as a nonpseudomorphic p-$Al_{0.38}Ga_{0.62}N$ bulk layer were compared. The total nominal thickness of the p-current spreading layer (150 nm), the magnesium supply, and the p^+-GaN cap (3D grown) were kept constant.

Figure 1 shows the associated values of the electroluminescence measurements at 20 mA. The LED wafers with the two different p-SLs show a similar output power and operating voltage of 0.88 mW and 5.4 V, respectively. However, the LED wafer with the bulk p-AlGaN current spreading layer exhibits

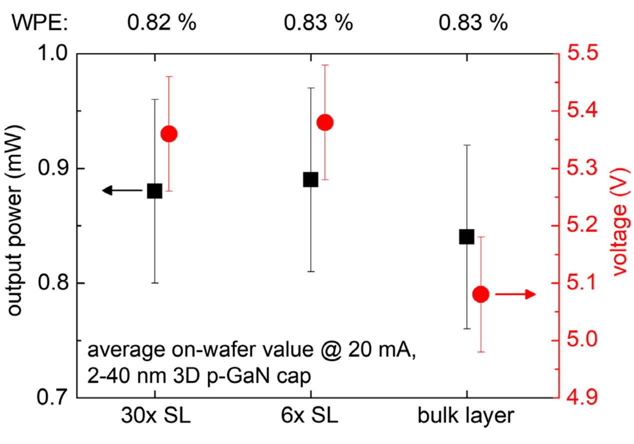

Figure 1. Output power and voltage of 310 nm LEDs with 30-period and 6-period p-$Al_{0.42}Ga_{0.58}N/Al_{0.32}Ga_{0.68}N$ SLs as well as a p-$Al_{0.38}Ga_{0.62}N$ bulk layer (each 150 nm thick) measured on wafers at 20 mA. On top of the figure, the wall plug efficiency (WPE) values calculated from the average output power and voltage are shown.

only a slightly lower average output power of 0.84 mW (with overlapping error bars to the SL samples) but also a lower operating voltage of 5.1 V. These results do not agree with findings from the literature that SLs yield a higher conductivity of the p-current spreading layer than a bulk layer as it was found for low-aluminum-content relaxed SLs.[22,24]

During the growth of the SLs, the in situ reflectometry at 405 nm did not indicate any surface roughening as a result of relaxation processes during nonpseudomorphic growth. To clarify the reason for the higher forward voltage, cross-sectional STEM was carried out on different LED heterostructures. The STEM image intensity increases with increasing gallium content and so provides a direct, qualitative assessment of composition across the SL. **Figure 2**a shows an exemplary STEM image of an LED heterostructure with a p-AlGaN layer of uniform composition. In addition, magnified images of the p-AlGaN region, marked by the dashed line in Figure 2a, are shown for different heterostructures: the 30-period p-AlGaN/AlGaN SPSL (Figure 2b), the 6-period p-AlGaN/AlGaN SL (Figure 2c), and the bulk p-AlGaN layer (Figure 2d). The cross-sectional STEM image of the nominally 30-period p-$Al_{0.42}Ga_{0.58}N/Al_{0.32}Ga_{0.68}N$ SPSL (Figure 2b) does not show the targeted SL periodicity. Instead, it shows partly nonperiodic layers with different thicknesses and varying STEM intensities, which indicate varying aluminum mole fractions between the individual layers. A conformity of the target and the real p-SL structure can be only observed in the top region near the p^+-GaN cap. Such variations in the thickness and composition of individual layers have so far not been reported in SLs with a high aluminum mole fraction, when the strain of the SL grown on AlN is lower. In contrast, for higher gallium contents, the formation of SLs with such disturbed periodicities and varying compositions takes place reproducibly. This fact suggests a stress-driven compositional change in our samples. The cross-sectional STEM image of the p-current spreading layer with a reduced number of SL periods (six periods) and a simultaneously increased period thickness is shown in Figure 2c. In this case an unintended self-organized periodic variation of the composition is formed in the layers with the higher aluminum mole fraction of the SL and the whole SL has a nonuniform period thickness (increase in layer thickness with low aluminum mole fraction and decrease in layer thickness with high aluminum mole fraction in growth direction). In contrast, in the case of the p-$Al_{0.38}Ga_{0.62}N$ bulk current spreading layer, the corresponding cross-sectional STEM image, in Figure 2d, shows nearly no intensity variations. This indicates growth of a uniform and reproducible p-AlGaN current spreading layer.

The observed self-organized compositional pulling during SL growth is known from the highly mismatched AlGaN wells on AlN or GaN templates[25] and even in pseudomorphic distributed Bragg reflectors,[26–28] if the gallium content is high, i.e., if there is strong compressive stress. One common explanation was that gallium adatoms with their large atomic radius are rejected at the growth front to minimize compressive stress.[25,29] Newer investigations[30,31] revealed that such compositional variations can be also triggered by the surface morphology, i.e., the substrate off-cut (the number and height of steps), species supersaturation (gallium coverage), and dislocation density. The effect can be prevented by ensuring uniform step-flow growth.[31] The explanation agrees with the observed decreasing

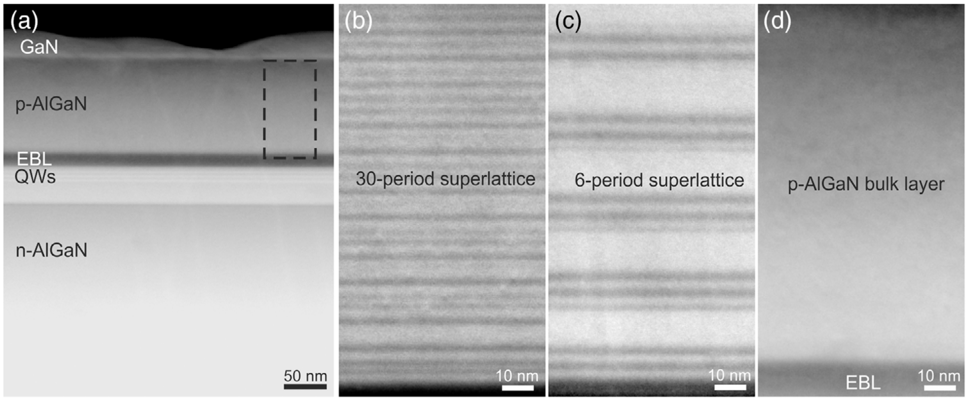

Figure 2. a) Exemplary cross-section STEM image of a 310 nm LED with magnified images of the p-AlGaN region for b) a nominal 30-period SPSL and c) a nominal 6-period p-$Al_{0.42}Ga_{0.58}N/Al_{0.32}Ga_{0.68}N$ SL as well as d) a p-$Al_{0.38}Ga_{0.62}N$ bulk layer.

compositional variations toward the p$^+$-GaN cap as the SL structure increasingly relaxes and variations of the growth rate disappear. The relaxation of the compressive stress of the SL layers is caused by the formation of new dislocations. All these effects may contribute to the fact that the forward voltage of LEDs with SLs as the p-current spreading layer is not lower than that of LEDs with a bulk layer and that it is unreproducible in contrast to the properties of the fully relaxed p-SLs reported in previous studies.[22,24] As the dislocations represent traps for holes, they can also reduce p-conductivity of the SLs.[12,32] In addition, due to the large thickness and composition fluctuations of the SL layers, the enhanced ionization of the magnesium acceptors by polarization fields doesn't take place which destroys the possibly better conductivity of a SL. Therefore, for further investigations of the p-side design, the p-doped SL in the 310 nm LEDs was replaced by a p-$Al_{0.38}Ga_{0.62}N$ bulk layer.

2.2. Thickness of p-AlGaN Bulk Layer

Based on the optimizations of the preceding paragraph, the thickness of the p-$Al_{0.38}Ga_{0.62}N$ bulk current spreading layer was reduced to investigate its influence on the output power and operating voltage. The rest of the LED heterostructure was kept constant.

Figure 3 shows the output power and operating voltage that depend on the p-AlGaN current spreading layer thickness. It was found that the output power increases by 40 % from 1.0 to 1.4 mW and the operating voltage decreases by 8 % from 6.3 to 5.8 V when decreasing the p-AlGaN current spreading layer thickness from 150 nm to 50 nm. The data show a large influence of the current spreading layer thickness on the electrical and optical characteristics of UV LEDs. The effect can be attributed to the high sheet resistance of the p-$Al_{0.38}Ga_{0.62}N$ layer, i.e., a large fraction of the operating voltage drops at this layer. This effect can be minimized with a reduced p-AlGaN layer thickness. The dependence of the output power on the layer thickness suggests that the hole injection is enhanced with a reduced p-AlGaN layer thickness because transmission measurements show that the p-AlGaN layer is transparent for the emitted 310 nm light, i.e., absorption effects can be excluded. Based

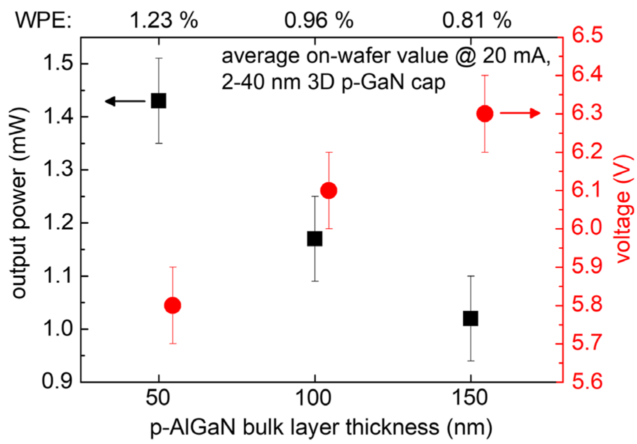

Figure 3. Output power and voltage of 310 nm LEDs with different p-$Al_{0.38}Ga_{0.62}N$ bulk layer thicknesses measured on wafers at 20 mA. On top of the figure the WPE values calculated from the average output power and voltage are shown.

on these results and better reproducibility of a p-AlGaN bulk current spreading layer growth, this p-layer heterostructure design is used for further optimizations. For thicknesses below 50 nm, a breakthrough of the LED was observed because a too thin p-AlGaN layer results in minor current spreading and hence a very high local current density.

2.3. p-GaN Cap Layer

After the optimization of the p-current spreading layer, the p$^+$-GaN cap layer was optimized. The highly magnesium-doped p-GaN cap layer is intended to support the realization of low-resistance p-metal contacts. Therefore, LED wafers with p$^+$-GaN cap layers grown under different conditions have been investigated.

The p$^+$-GaN cap grown in a 3D growth mode consists of islands for the use of reflective metal contacts (see the bird's-eye view SEM image in **Figure** 4a). Cross-sectional STEM reveals a variation of the p-GaN layer thickness between

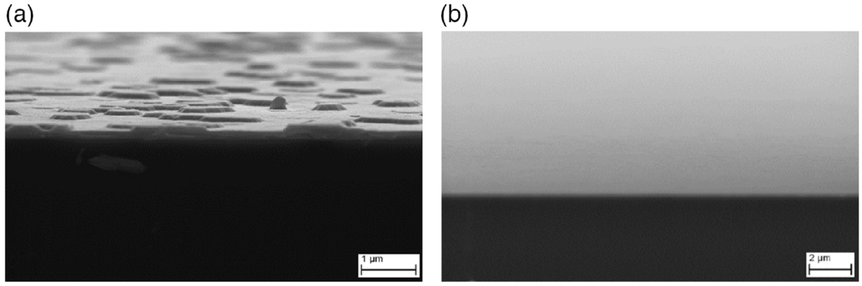

Figure 4. SEM images taken as a bird's eye view of epitaxial structures for 310 nm LEDs with a) 3D island-grown and b) 2D-grown p^+-GaN cap layer.

2 nm (in the valley area) and 40 nm of the islands. The 3D growth is attributed to the strong compressive stress of the p^+-GaN layer on the p-$Al_{0.38}Ga_{0.62}N$ current spreading layer. Most likely, the GaN island growth starts at nuclei at the surface formed by the end points of dislocation lines or some other morphological disturbances. This results in an inhomogeneous coverage of the surface with p^+-GaN in the form of islands which coalesce only at much larger layer thicknesses of 150 nm and beyond (not shown in this article). A big disadvantage of a thick p-GaN cap layer is reduced output power because of its strong UVB light absorption. In contrast, an uncovered p-AlGaN contact layer would be best as it avoids any absorption but it would also result in high-resistance p-contacts and high operation voltages. To find a good compromise between output power and operating voltage, the growth conditions and the thickness of the p^+-GaN cap layer were varied. Therefore, LEDs with a p^+-GaN cap grown with a strongly reduced 3D growth have been fabricated. The SEM image of the smooth wafer surface, as shown in Figure 4b, shows a much better wettability compared with the 3D grown cap and confirms this approach. By a variation of the growth time, two samples with nearly uniform layer thicknesses of (18 ± 5) nm and (35 ± 5) nm can be compared.

The corresponding output power and operating voltage measured at 20 mA are shown in **Figure 5**. LEDs with a non-uniform p^+-GaN cap layer, which consists of islands, show the highest output power and highest operating voltage of 1.22 mW and 5.24 V, respectively. This is due to low absorption and partial reflection at the metal contacts in the areas of a thin p-GaN cap, on the one hand, and only limited areas with a low contact resistivity in the areas of a thick p^+-GaN cap, on the other hand. In contrast, the LEDs with the smooth and closed p^+-GaN cap layer show a lower operating voltage (below 5 V) because the uniform p^+-GaN layer results in a uniformly low contact resistivity. In contrast, the output power is reduced presumably by the increased absorption of UVB light in the uniform p^+-GaN cap layer. The output power of LEDs with the 35 nm p^+-GaN cap layer is reduced by around 34% (0.81 mW) compared to the LEDs with p^+-GaN islands. In this case, a reduction of the absorbing p^+-GaN layer thickness leads to an increase in output power, which can be observed for LEDs with half the thickness of the uniform p^+-GaN cap layer. These LEDs show an increased output power of 1.05 mW, which is a reduction of only around 14% in comparison to the LEDs with the 3D p^+-GaN cap. A further reason for the higher output power of LEDs with a nonuniform cap layer could be also a local higher carrier concentration in the p^+-GaN islands, which may shift the recombination dynamics toward a higher radiative recombination efficiency at same nominal current density. In addition, the reduction of the thickness of the presumably highly resistive uniform p^+-GaN layer leads to a lower forward voltage at unchanged low contact resistivity. A further reduction in the layer thickness showed an increase in contact resistivity, as magnesium concentration in the topmost part of the layer is too low ($< 2 \times 10^{20}$ cm^{-3}), as magnesium has to accumulate at the surface during growth before its incorporation is maximum (not shown in this article).

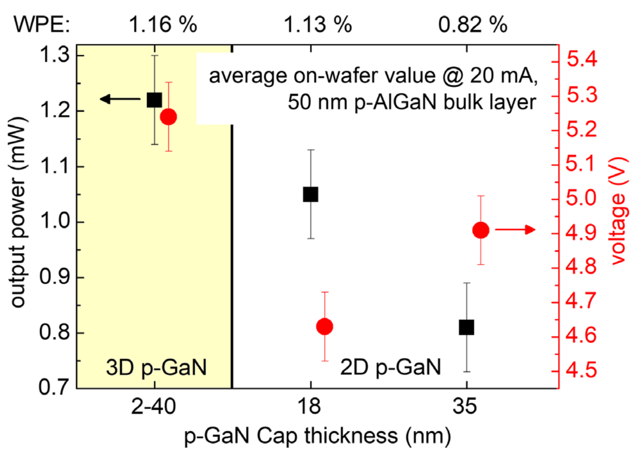

Figure 5. Output power and voltage of 310 nm LEDs with different p^+-GaN cap layers measured on wafers at 20 mA. On top of the figure the WPE values calculated from the average output power and voltage are shown.

3. Conclusion

The influence of the design and the thickness of the p-AlGaN current spreading layer as well as the growth conditions and thickness of the p^+-GaN cap layer on the emission characteristics of 310 nm LEDs have been investigated. Nonpseudomorphic p-AlGaN SLs are proposed to enhance the hole injection and increase vertical conductivity. However, self-organized vertical variations of the SL composition were observed. This led to unreproducible properties of the SLs and increased the LED forward voltages in comparison with LEDs with bulk p-AlGaN as current spreading layer. Using a uniform p-AlGaN bulk layer, the

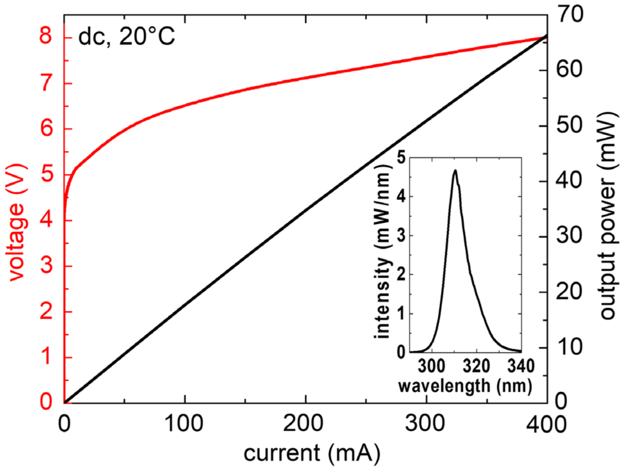

Figure 6. Electrical and optical characteristics of a flip-chip-mounted 310 nm LED measured under DC. Inset: the corresponding emission spectrum measured at 350 mA.

corresponding LEDs show a slightly lower output power but also a lower operating voltage. A thinner p-AlGaN bulk current spreading layer increases the output power and decreases the operating voltage. Finally, LEDs with a nonuniform p^+-GaN cap layer, which consists of islands, feature the highest output power but also the highest operating voltage. In contrast, the output power and the operating voltage of LEDs with a smooth and closed p^+-GaN cap depend on the thickness of the cap, which can be attributed to its absorption and limited conductivity.

Based on a combination of all these optimization steps, flip-chip-mounted 310 nm LEDs with an output power of 59 mW and an operating voltage of 7.8 V at an operation current of 350 mA were realized. The corresponding electrical and optical characteristics as well as the emission spectrum are shown in **Figure 6**.

4. Experimental Section

The LED heterostructures were grown on 2 in. (0001)-oriented sapphire substrates by metal-organic vapor phase epitaxy (MOVPE) in a Thomas Swan 6×2 in. closed coupled showerhead reactor equipped with in situ metrology. Trimethylaluminum, trimethylgallium, triethylgallium, trimethylindium, ammonia, disilane, and biscyclopentadienylmagnesium were used as source materials. After the deposition of a 1600 nm-thick AlN layer at an elevated temperature, a 200 nm AlN/GaN SPSL was grown, followed by a 500 nm undoped and 4.5 μm silicon-doped $Al_{0.55}Ga_{0.45}N$ contact layer, a threefold (In)AlGaN/(In)AlGaN multiple QW active region, a 16 nm-thick Mg-doped EBL, a p-current spreading layer, and a heavily magnesium-doped GaN contact layer as cap. The AlN base layer on sapphire showed a typical full width at half maximum of the omega X-ray rocking curves of 80 arcsec for the (00.2) reflection and 550 arcsec for the (10.2) reflection. The corresponding threading dislocation density was about $(3-4) \times 10^9$ cm^{-2}.[33,34] The dislocation density in the active region, determined by counting the dark spot density in monochromatic cathodoluminescence images of the QWs, was $(1-2) \times 10^9$ cm^{-2}. The layer thicknesses were determined by in situ reflectometry and SEM or STEM on the cross section of the device structures. The degree of relaxation and layer compositions were determined by high-resolution X-ray diffraction (HRXRD), using $\omega - \omega/2\theta$ reciprocal space maps (RSM) of the (00.4) and (11.4) reflections as well as XRD omega rocking curves of the (00.2) and (10.2) reflection in a Malvern PANanalytical X'Pert3 system. For rocking curve measurements, the aperture on the source side was 0.5 mm $\times$ 5 mm and the acceptance angle in front of the detector was 1°. For RSM measurements, an array detector was used.

In a first series of samples, the influence of the p-current spreading layer design was investigated. Therefore, LEDs with a nominal 30-period (2.5 nm/2.5 nm) or 6-period (12.5 nm/12.5 nm) p-$Al_{0.42}Ga_{0.58}N/Al_{0.32}Ga_{0.68}N$ SL as well as a p-$Al_{0.38}Ga_{0.62}N$ bulk layer were compared. The nominal magnesium doping level and the total thickness of the current spreading layer of all samples were kept constant at 2×10^{19} cm^{-3} and 150 nm, respectively. The layer composition and growth rate of the AlGaN layers used for SLs were determined at bulk layers on calibration samples. Due to the large lattice mismatch, the p^+-GaN cap layer grew in a 3D island mode with thickness fluctuations of 2–40 nm.

In a second series of samples, the thickness of the p-$Al_{0.38}Ga_{0.62}N$ bulk layer was reduced. LEDs with 150, 100, or 50 nm p-$Al_{0.38}Ga_{0.62}N$ bulk layers and a 2–40 nm 3D p^+-GaN cap layer were analyzed.

Finally, in a third set of samples, the growth conditions and the thickness of the p^+-GaN cap layer were varied based on the LED heterostructure with a 50 nm p-$Al_{0.38}Ga_{0.62}N$ bulk layer. LEDs with a 2–40 nm-thick 3D p^+-GaN cap layer were compared with LEDs with 2D-grown p^+-GaN cap layers with thicknesses of 18 and 35 nm, respectively.

After MOVPE growth, the samples were annealed in nitrogen ambient to activate Mg dopants. LEDs were fabricated using standard chip-processing technologies. Mesa structures were defined by inductively coupled plasma etching to expose the n-AlGaN surface. Platinum-based p-contacts and vanadium–aluminum-based n-contacts were deposited to form the p-electrode and the n-electrode, respectively.

The electrical and optical characteristics of the LEDs were measured on wafers under direct current (DC) injection. For that purpose, the wafers were placed episide up on a sample holder without any active cooling. The emission spectra and the optical power versus current (*L–I*) characteristics were measured by collecting the light emitted through the substrate with an optical fiber spectrometer and a calibrated silicon photodiode, respectively. In addition, cross-sectional STEM and SEM measurements of the LED heterostructures were used to explain the observations more in detail.

Acknowledgements

The authors thank C. Neumann and T. Petzke for technical MOVPE support and H. Lawrenz for SEM measurements. This work was partially supported by the German Federal Ministry of Education and Research (BMBF) through the consortia project "Advanced UV for Life" under the contract 03ZZ0134B. Open access funding enabled and organized by Projekt DEAL.

Conflict of Interest

The authors declare no conflict of interest.

Keywords

light-emitting diode heterostructures, metal-organic vapor phase epitaxies, p-current spreading layers, p-GaN cap layers, ultraviolet light-emitting diodes

Received: June 29, 2020
Revised: August 5, 2020
Published online: September 9, 2020

[1] K. Davitt, Y. Song, W. R. Patterson III, A. Nurmikko, M. Gherasimova, J. Han, Y. Pan, R. G. Chang, *Opt. Express* **2005**, *13*, 9548.

[2] M. Kneissl, J. Rass, *Springer Series In Materials Science 227, III-Nitride Ultraviolet Emitters – Technology And Applications*, Springer, New York **2016**.
[3] M. Shatalov, W. Sun, R. Jain, A. Lunev, X. Hu, A. Dobrinsky, Y. Bilenko, J. Yang, G. A. Garrett, L. E. Rodak, M. Wraback, M. Shur, R. Gaska, *Semicond. Sci. Technol.* **2014**, *29*, 084007.
[4] M. S. Shur, *IEEE Trans. Electron Dev.* **2010**, *57*, 12.
[5] J.-S. Park, J. K. Kim, J. Cho, T. Y. Seong, *ECS J. Solid State Sci. Technol.* **2017**, *6*, Q42.
[6] M. Kneissl, T. Kolbe, C. Chua, V. Küller, N. Lobo, J. Stellmach, A. Knauer, H. Rodriguez, S. Einfeldt, Z. Yang, N. M. Johnson, M. Weyers, *Semicond. Sci. Technol.* **2011**, *26*, 014036.
[7] C. Chu, K. Tian, Y. Zhang, W. Bi, Z.-H. Zhang, *Phys. Status Solidi A* **2019**, *216*, 1800815.
[8] T. Takano, T. Mino, J. Sakai, N. Noguchi, K. Tsubaki, H. Hirayama, *Appl. Phys. Express* **2017**, *10*, 031002.
[9] J. Zhang, Y. Gao, L. Zhou, Y.-U. Gil, K.-M. Kim, *Semicond. Sci. Technol.* **2018**, *33*, 07LT01.
[10] Y. Nagasawa, A. Hirano, *Appl. Sci.* **2018**, *8*, 1264.
[11] M. Kneissl, T.-Y. Seong, J. Han, H. Amano, *Nat. Photonics* **2019**, *13*, 233.
[12] A. Knauer, T. Kolbe, J. Rass, H. K. Cho, C. Netzel, S. Hagedorn, N. Lobo Ploch, J. Ruschel, J. Glaab, S. Einfeldt, M. Weyers, *Jpn. J. Appl. Phys.* **2019**, *58*, SCCC02.
[13] A. Knauer, H. Wenzel, T. Kolbe, S. Einfeldt, M. Weyers, M. Kneissl, G. Tränkle, *Appl. Phys. Lett.* **2008**, *92*, 191912.
[14] T. Kolbe, T. Sembdner, A. Knauer, V. Küller, H. Rodriguez, S. Einfeldt, P. Vogt, M. Weyers, M. Kneissl, *Phys. Status Solidi C* **2010**, *7*, 2196.
[15] T. Kolbe, T. Sembdner, A. Knauer, V. Küller, H. Rodriguez, S. Einfeldt, P. Vogt, M. Weyers, M. Kneissl, *Phys. Status Solidi A* **2010**, *207*, 2198.
[16] T. Kolbe, J. Stellmach, F. Mehnke, M.-A. Rothe, V. Küller, A. Knauer, S. Einfeldt, T. Wernicke, M. Weyers, M. Kneissl, *Phys. Status Solidi A* **2016**, *213*, 210.
[17] T. Kolbe, A. Knauer, J. Rass, H. K. Cho, S. Hagedorn, S. Einfeldt, M. Kneissl, M. Weyers, *Materials* **2017**, *10*, 1396.
[18] C. Pernot, M. Kim, S. Fukahori, T. Inazu, T. Fujita, Y. Nagasawa, A. Hirano, M. Ippommatsu, M. Iwaya, S. Kamiyama, I. Akasaki, H. Amano, *Appl. Phys. Express* **2010**, *3*, 061004.
[19] K. X. Chen, Y. A. Xi, F. W. Mont, J. K. Kim, E. F. Schubert, W. Liu, X. Li, J. A. Smart, *J. Appl. Phys.* **2007**, *101*, 113102.
[20] G. F. Yang, F. Xie, K. X. Dong, P. Chen, J. J. Xue, T. Zhi, T. Taoa, B. Liu, Z. L. Xie, X. Q. Xiu, P. Han, Y. Shi, R. Zhang, Y. D. Zheng, *Phys. E* **2014**, *62*, 55.
[21] M. A. Khan, N. Maeda, M. Jo, Y. Akamatsu, R. Tanabe, Y. Yamadaband, H. Hirayama, *J. Mater. Chem. C* **2019**, *7*, 143.
[22] A. A. Allermann, M. H. Crawford, M. A. Miller, S. R. Lee, *J. Cryst. Growth* **2010**, *312*, 756.
[23] K. Ebata, J. Nishinaka, Y. Taniyasu, K. Kumakura, *Jpn. J. Appl. Phys.* **2018**, *57*, 04FH09.
[24] K. Sato, S. Yasue, Y. Ogino, M. Iwaya, T. Takeuchi, S. Kamiyama, I. Akasaki, *Jpn. J. Appl. Phys.* **2019**, *58*, 1016.
[25] B. Liu, R. Zhang, J. G. Zheng, X. L. Ji, D. Y. Fu, Z. L. Xie, D. J. Chen, P. Chen, R. L. Jiang, Y. D. Zheng, *Appl. Phys. Lett.* **2011**, *98*, 261916.
[26] C. He, Z. Qin, F. Xu, L. Zhang, J. Wang, M. Hou, S. Zhang, X. Wang, W. Ge, B. Shen, *Sci. Rep.* **2016**, *6*, 25124.
[27] H. Y. Lin, Y. F. Chen, T. Y. Lin, C. F. Shih, K. S. Liu, N. C. Chen, *J. Cryst. Growth* **2006**, *290*, 225.
[28] Y.-S. Liu, S. Wang, H. Xie, T.-T. Kao, K. Mehta, X. J. Jia, S.-C. Shen, P. D. Yoder, F. A. Ponce, T. Detchprohm, *Appl. Phys. Lett.* **2016**, *109*, 081103.
[29] N. Grandjean, J. Massies, M. Leroux, *Phys. Rev. B* **1996**, *53*, 998.
[30] I. Bryan, Z. Bryan, S. Mita, A. Rice, L. Hussey, C. Shelton, J. Tweedie, J.-P. Maria, R. Collazo, Z. Sitar, *J. Cryst. Growth* **2016**, *451*, 65.
[31] J. H. Dycus, S. Washiyama, T. B. Eldred, Y. Guan, R. Kirste, S. Mita, Z. Sitar, R. Collazo, J. M. LeBeau, *Appl. Phys. Lett.* **2019**, *114*, 031602.
[32] I. Bryan, Z. Bryan, S. Washiyama, P. Reddy, B. Gaddy, B. Sarkar, M. H. Breckenridge, Q. Guo, M. Bobea, J. Tweedie, S. Mita, D. Irving, R. Collazo, Z. Sitar, *Appl. Phys. Lett.* **2018**, *112*, 062102.
[33] T. Metzger, R. Höpler, E. Born, O. Ambacher, M. Stutzmann, R. Stömmer, M. Schuster, H. Göbel, S. Christiansen, M. Albrecht, H. P. Strunk, *Philos. Mag. A* **1998**, *77*, 1013.
[34] H. Heinke, V. Kirchner, S. Einfeldt, D. Hommel, *Phys. Status Solidi A* **1999**, *176*, 391.